Available online at www.sciencedirect.com
ScienceDirect
Proceedings of the Combustion Institute 32 (2009) 1937–1945
Proceedings of the Combustion Institute
www.elsevier.com/locate/proci

Hetero-/homogeneous combustion of hydrogen/air mixtures over platinum at pressures up to 10 bar

John Mantzaras *, Rolf Bombach, Rolf Schaeren

Paul Scherrer Institute, Combustion Research, CH-5232 Villigen PSI, Switzerland

Abstract

The hetero-/homogeneous combustion of fuel-lean hydrogen/air premixtures over platinum was investigated experimentally and numerically in the pressure range 1 bar $\leqslant p \leqslant$ 10 bar. Experiments were carried out in an optically accessible channel-flow catalytic reactor and included planar laser induced fluorescence (LIF) of the OH radical for the assessment of homogeneous (gas-phase) ignition, and 1-D Raman measurements of major gas-phase species concentrations for the evaluation of the heterogeneous (catalytic) processes. Simulations were performed with a full-elliptic 2-D model that included detailed heterogeneous and homogeneous chemical reaction schemes. The predictions reproduced the measured catalytic hydrogen consumption, the onset of homogeneous ignition at pressures of up to 3 bar and the diminishing gas-phase combustion at $p \geqslant 4$ bar. The suppression of gaseous combustion at elevated pressures bears the combined effects of the intrinsic homogeneous hydrogen kinetics and of the hetero/homogeneous chemistry coupling via the catalytically produced water over the gaseous induction zone. Transport effects, associated with the large diffusivity of hydrogen, have a smaller impact on the limiting pressure above which gaseous combustion is suppressed. It is shown that for practical reactor geometrical confinements, homogeneous combustion is still largely suppressed at $p \geqslant 4$ bar even for inlet and wall temperatures as high as 723 and 1250 K, respectively. The lack of appreciable gaseous combustion at elevated pressures is of concern for the reactor thermal management since homogeneous combustion moderates the superadiabatic surface temperatures attained during the heterogeneous combustion of hydrogen.

Keywords: Hetero-/homogeneous high-pressure hydrogen combustion; Platinum catalyst; In situ Raman and laser induced fluorescence; Suppression of homogeneous ignition

1. Introduction

The need to reduce greenhouse CO_2 emissions from large power plants has led to increased interest for fuel decarbonization technologies that yield hydrogen-rich reformed fuels [1]. In addition, microreactors using hydrogen or hydrogen enriched fuels are a promising route for portable production of energy and heat [2,3]. While catalytic combustion is an option for large-scale power generation [4] and also for household power/heat production, it is

* Corresponding author. Fax: +41 56 3102199.
E-mail address: ioannis.mantzaras@psi.ch (J. Mantzaras).

1540-7489/$ - see front matter © 2009 The Combustion Institute. Published by Elsevier Inc. All rights reserved.
doi:10.1016/j.proci.2008.06.067

the preferred route for microreactors [5–7] due to their associated large surface-to-volume ratios.

In the last years there is an intensification of experimental studies aiming at improving the understanding of homogeneous kinetics for hydrogen and hydrogen-rich syngas fuels at elevated pressures [8,9]. On the other hand, there is a lack of corresponding high-pressure hetero-/homogeneous combustion experiments for hydrogen or hydrogen-rich fuels. It is emphasized that although typical catalytic reactors have sufficiently large surface-to-volume ratios so as to promote heterogeneous fuel conversion, the contribution of gaseous chemistry cannot always be ignored, particularly in high-pressure hydrocarbon combustion [10,11]. To facilitate hetero-/homogeneous combustion studies, we have introduced the methodology of in situ spatially resolved Raman measurements of major gas-phase species concentrations and laser induced fluorescence (LIF) of radicals over the catalyst boundary layer as a direct way to assess the catalytic and gas-phase reactivities at realistic pressures and temperatures [10,12–14]. Appel et al. [14] provided validated hetero-/homogeneous reaction schemes for fuel-lean combustion of H_2/air over Pt catalysts at atmospheric pressure and clarified the underlying hetero-/homogeneous chemistry coupling. Subsequent studies furnished refined hetero-/homogeneous reaction schemes for the total oxidation of fuel-lean CH_4/air and $CH_4/O_2/H_2O/CO_2$ mixtures over Pt at pressures of up to 16 bar [10,13,15], and also for the partial oxidation of methane over Rh at pressures of up to 10 bar [16].

The present study undertakes a combined experimental and numerical investigation of fuel-lean hydrogen/air catalytic combustion over Pt at pressures $1\ \text{bar} \leqslant p \leqslant 10\ \text{bar}$. The range up to ~5 bar is of interest for portable power generation using micro-turbine concepts [7], while the upper end of 10 bar pertains to small gas turbines. The main objectives are to investigate the impact of pressure on homogeneous ignition and on the hetero-/homogeneous chemistry coupling, and to provide validated hetero-/homogeneous reaction schemes over the investigated pressure range.

Experiments have been performed in an optically accessible channel-flow catalytic reactor coated with platinum. The onset of homogeneous ignition was determined with planar laser induced fluorescence (LIF) of the OH radical, while the catalytic processes were monitored with one-dimensional Raman measurements of major gas-phase species concentrations. The numerical predictions included an elliptic 2-D model with detailed heterogeneous and homogeneous chemical reaction schemes.

2. Experimental

2.1. High-pressure test-rig

The test-rig included a channel-flow catalytic reactor, which was mounted inside a pressure-controlling cylindrical tank (see Fig. 1 and [10,13,16]). The reactor comprised two horizontal Si[SiC] ceramic plates (300 mm long (x), 110 mm wide (z), 9 mm thick, positioned 7 mm apart (y)) and two 3 mm thick vertical quartz windows (Fig. 1). The inner ceramic plate surfaces were coated via plasma vapor deposition with a 1.5 μm thick nonporous Al_2O_3 layer, followed by a 2.2 μm thick Pt layer. Measurements of the total and active catalyst surface areas with BET (Kr-physisorption) and CO-chemisorption, respectively, have verified the absence of surface porosity [13]. The surface temperature along the x–y symmetry plane was measured by S-type thermocouples (12 for each plate) embedded 0.9 mm beneath the catalyst surface through holes eroded from the outer Si[SiC] surfaces.

In fuel-lean catalytic combustion of diffusionally imbalanced fuels with Lewis numbers (Le) less than unity (in hydrogen $Le \sim 0.3$) superadiabatic surface temperatures are attained at the channel entry [11,14,17]. Similarly to our previous atmospheric pressure studies [14,18], a cooling/heating arrangement has been adopted to suppress the high entry surface temperatures and at the same time to balance the heat losses at the rear of the channel. To this direction, the front face of the channel was contacted to a water-cooled metal frame (see Fig. 1), while over the $100 < x < 300$ mm length two resistive heaters were positioned above the ceramic plates. Therefore, the established surface temperatures reflected the

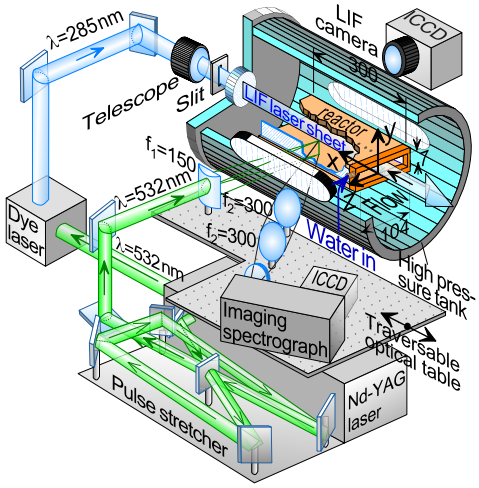

Fig. 1. Schematic of the test-rig and the Raman/LIF set-up.

combined effects of external heating/cooling and reaction exothermicity.

Compressed air was mixed with hydrogen in two sequential static mixers. The H_2/air premixture was directed to the reactor inlet via a 50-mm long inert rectangular honeycomb section (1×1 mm^2 channels), which yielded a uniform inlet velocity profile. A thermocouple positioned at the downstream end of the honeycomb monitored the reactor inlet temperature. Optical accessibility from both reactor sides was maintained with two 350-mm long and 35-mm thick quartz windows on the high-pressure tank (see Fig. 1). Two additional quartz windows, one located at the rear flange of the tank and the other (not shown in Fig. 1) at the reactor exhaust, provided a counterflow axial optical access for the LIF experiments.

2.2. Laser diagnostics

The Raman and LIF set-up is depicted in Fig. 1. A traversable mirror directed the 532 nm radiation of a frequency doubled Nd:YAG pulsed laser (Quantel YG981E20CL, 380 mJ pulse energy, 12 ns pulse) to the Raman or to the LIF set-up. In the Raman experiments, the 532 nm beam was temporally stretched to 34 ns using an optical delay line (Fig. 1). This allowed for efficient use of the entire pulse energy without window damage or dielectric gas breakdown. The temporally stretched beam was focused through the tank and reactor side-windows into a vertical line (~0.3 mm thick) by an $f_1 = 150$ mm cylindrical lens. The focal line spanned the entire 7 mm channel height and was laterally offset ($z = 15$ mm) to increase the light collection angle and minimize thermal beam steering [10]. Two $f_2 = 300$ mm spherical lenses focused the scattered light to the entrance slit of a 25-cm imaging spectrograph (Chromex-250i). The dispersed light was recorded on an intensified CCD camera (Princeton Instruments MAX-1024HQ, 1024×254 pixels). The 7 mm height was resolved with 200 pixels, which were further binned to 84 pixels. A holographic notch-filter (Kaiser HNPF-532.0-1.5) and a colored glass filter were placed before the spectrograph slit to attenuate the scattered Rayleigh signal and the stray laser light. The spectral dispersion extended up to 4500 cm^{-1}, allowing observation of all major species. Given the steady and laminar operating conditions, 4000 images were averaged to increase the signal-to-noise ratio. Measurements were acquired over the length 18 mm $\leqslant x \leqslant$ 150 mm by traversing axially an optical table that supported both sending and collecting optics (Fig. 1). Raman data closer than 0.5 mm to both walls were discarded due to low signal-to-noise ratios arising from the hot-wall thermal radiation interferences. The measurement accuracy was $\pm 3\%$ for species volumetric compositions $\geqslant 10\%$ and $\pm 10\%$ for compositions as low as 0.5% vol., while concentrations less than 0.5% vol. could not be accurately resolved.

For the OH-LIF, the 532-nm radiation pumped a tunable dye laser (Quantel TDL90 NBP2UVT3); its frequency-doubled radiation (285 nm) had a low pulse energy (~0.5 mJ) to avoid saturation of the $A(v = 1) \leftarrow X(v' = 0)$ transition. The 285 nm beam was transformed into a laser sheet (by a cylindrical lens telescope and a 1-mm slit mask) that propagated counterflow, along the x–y symmetry plane (Fig. 1). The fluorescence of both (1–1) and (0–0) transitions at 308 and 314 nm, respectively, was collected at 90° through the reactor and tank side-windows with an intensified CCD camera (LaVision-IRO with 1392×1024 pixels). Channel areas of 100×7 mm^2 were recorded on a 696×44 pixel section and the camera was traversed axially to map the entire reactor extent. At each measuring location, 400 images were averaged. The LIF was calibrated with absorption measurements performed with the 285 nm beam crossing the flames laterally (z direction) through both side windows, as in [10,12]; this was possible only for pressures $p \leqslant 3$ whereby strong flames were established in the channel. Details of the Raman and LIF set-up have been provided elsewhere [10,13,16].

3. Numerical

A full-elliptic 2-D CFD code was used in the simulations [10,13]. The computational domain comprised 200 mm $\times$ 7 mm (in x and y, respectively) since the resulting flames were located within the initial 200 mm reactor length. An orthogonal staggered grid of 400×120 grid points (in x and y, respectively) was sufficient to produce a grid independent solution. Uniform profiles for the temperature, the axial velocity and the species mass fractions were used at the inlet. Fitted curves through the individual thermocouple measurements provided the bottom-wall and top-wall temperature profiles, which served as energy boundary conditions at $y = 0$ and 7 mm, respectively. No-slip conditions for both velocity components were applied at the channel walls and zero-Neumann conditions at $x = 200$ mm.

The elementary heterogeneous reaction scheme of Deutschmann et al. [19] (11 irreversible and three reversible reactions, 5 surface and 6 gaseous species) was employed; surface thermodynamic data for the reversible reactions were taken from [20]. The platinum surface site density was 2.7×10^{-9} mol/cm^2 [19]. For gaseous hydrogen chemistry, the scheme of Li et al. [8] was used (21 reversible reactions and 9 species); gas-phase thermodynamic data were also provided therein [8]. This mechanism has been validated against

shock tube and laminar flame speed measurements at pressures up to 87 bar. gas-phase and surface reaction rates were evaluated with CHEMKIN [21] and Surface-CHEMKIN [22], respectively. Mixture-average diffusion, including thermal diffusion for the light species H and H_2, was used in conjunction with the CHEMKIN transport database [23].

4. Results and discussion

Experiments were carried out for two H_2/air stoichiometries, $\varphi = 0.28$ and 0.32, and two inlet Reynolds numbers (based on the uniform incoming properties and the channel hydraulic diameter), $Re_{IN} = 1000$ and 2000, that yielded laminar flows. Recent turbulent catalytic combustion studies [18] have actually shown that the strong flow laminarization induced by the hot catalytic walls guarantees laminar conditions at Re_{IN} considerably higher than 2000. The inlet temperature was in all cases 310 K and the surface temperatures ranged between 1080 and 1248 K. For a given set of measurements, the inlet velocity (U_{IN}) was reduced with rising pressure so as to maintain the same Re_{IN}. This procedure facilitated comparison of the gaseous reactivity at different pressures: analytical studies have shown [24] that for a given Re_{IN} and mass-transport-limited catalytic fuel conversion, the homogeneous ignition distance is controlled by the gaseous reactivity (all other parameters being the same, i.e. wall temperature, inlet temperature, channel geometry).

4.1. Homogeneous ignition

Comparisons between measured and predicted OH distributions (ppmv) are illustrated in Fig. 2

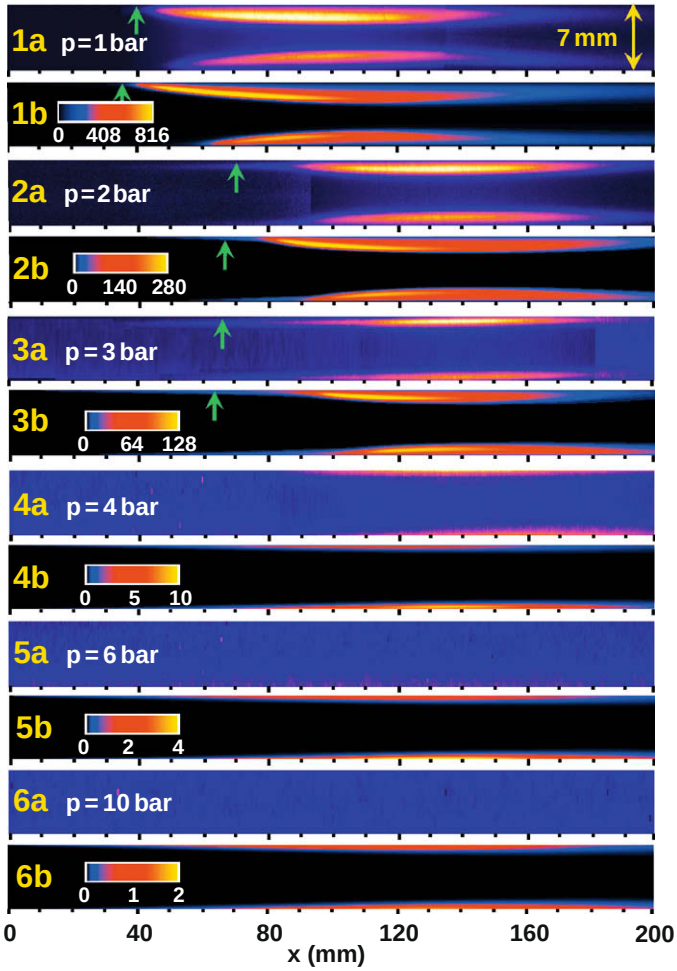

Fig. 2. (a) LIF-measured and (b) numerically predicted OH maps for a $\varphi = 0.28$ H_2/air mixture at various pressures. The inlet Reynolds number is 2000 in all cases. The arrows in Cases 1 to 3 define the onset of homogeneous ignition. The provided scales in the color bars span the minimum and maximum predicted OH in ppmv.

for $\varphi = 0.28$, $Re_{IN} = 2000$ (corresponding to $U_{IN} = 3$ m/s at $p = 1$ bar) and six different pressures. The measured OH distributions have been constructed by using overlapping 100 mm long LIF images. Similar graphs for $\varphi = 0.32$ and/or $Re_{IN} = 1000$, lead to the same conclusions as in the base study of Fig. 2, and are not presented herein. The flames of Fig. 2 exhibit a moderate asymmetry due to temperature differences between the two walls, the upper wall being typically hotter than the lower one over the initial 80 mm channel length (see Fig. 3). The position of homogeneous ignition (x_{ig}), shown with the green arrows in Fig. 2 for all the $p \leqslant 3$ bar flames, has been defined in both predictions and experiments as the far upstream location where OH reaches 5% of its maximum value in the reactor. The maximum OH levels decrease with rising pressure as seen in Fig. 2. The experimentally measured maximum OH levels for Cases 1 to 3 ($p \leqslant 3$ bar, wherein calibration via OH absorption was possible), were within 20% of the predicted values. While for Case 4 ($p = 4$ bar) a weak OH signal could still be measured, for higher pressures no OH signal could be detected above the thermal radiation noise of the hot catalytic plates, even at the highest gain of the ICCD camera. The maximum predicted OH at 6 and 10 bar (3.8 and 1.6 ppmv, respectively) were too low for detection with planar LIF, when also considering the aforementioned interference from the hot walls.

The comparisons of Fig. 2 are quite favorable in terms of flame shapes, homogeneous ignition distances for $p \leqslant 3$ bar, and diminishing OH levels for $p \geqslant 4$ bar. The latter signify that gaseous combustion is largely suppressed at $p \geqslant 4$ bar, and this is further confirmed by the Raman measurements. Comparisons between Raman-measured and predicted transverse profiles of the H_2 and H_2O mole fractions are shown in Fig. 4 for three cases of Fig. 2 and two axial positions, $x = 28$ and 108 mm. The Raman measurements are crucial in assessing the catalytic processes preceding homogeneous ignition. An incorrect prediction of the upstream catalytic fuel conversion can significantly affect homogeneous ignition [11] and may thus falsify the gaseous kinetics. The Raman profiles at the upstream position $x = 28$ mm (Fig. 4a) indicate a catalytic conversion close to the mass-transport-limit (shown by the very low hydrogen levels near both walls), irrespective of pressure. This behavior is captured well by the employed catalytic scheme [19]. The presence of gaseous combustion at $x = 108$ mm for the 1 bar

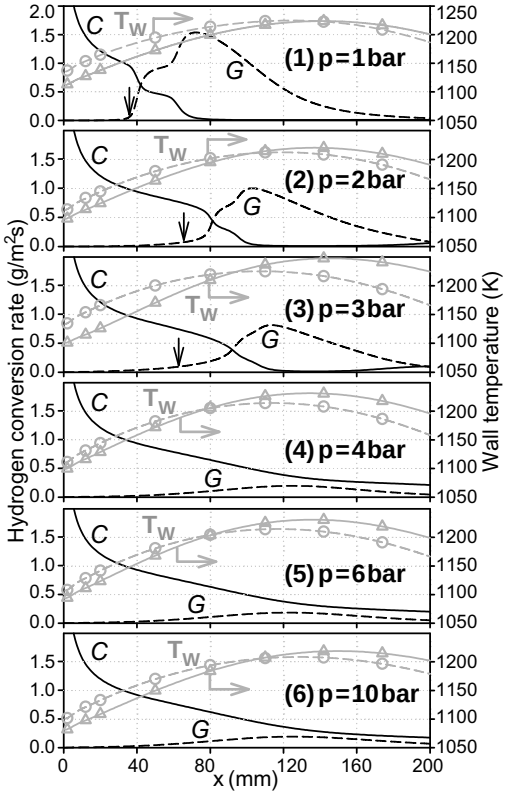

Fig. 3. Temperature profiles of upper-wall (dashed gray lines) and lower-wall (solid gray lines), fitted through the thermocouple measurements (upper-wall: circles; lower-wall: triangles) for all cases of Fig. 2. The computed catalytic (C) and gas-phase (G) hydrogen conversions are shown with solid and dashed black lines, respectively. The arrows in Cases 1 to 3 define the onset of homogeneous ignition.

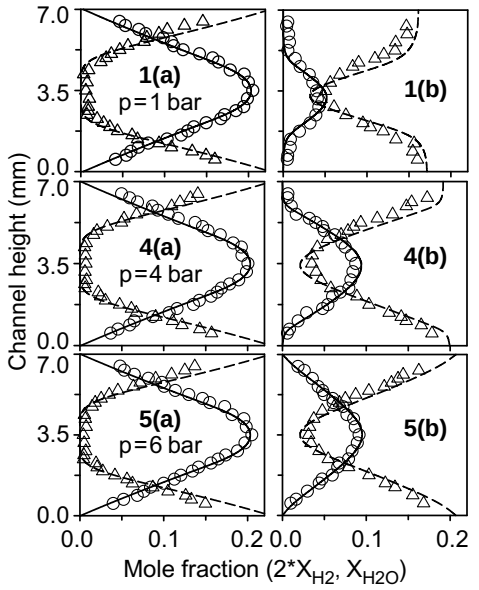

Fig. 4. Measured (symbols) and predicted (lines) species transverse profiles for three cases of Fig. 2: H_2 (solid lines, circles), H_2O (dashed-lines, triangles). The axial positions are: (a) $x = 28$ mm and (b) $x = 108$ mm.

case is manifested by the absence of H_2 and the presence of H_2O in extended zones near both walls (Fig. 4(1b)). At $p = 4$, the near-wall gaseous combustion zones become considerably narrower (Fig. 4(4b)) and they practically vanish at $p = 6$ bar (Fig. 4(5b)).

Streamwise profiles of the computed catalytic (C) and gaseous (G) hydrogen consumption rates (the latter integrated over the 7 mm channel-height) are also provided in Fig. 3 for all cases of Fig. 2. The sudden rise of the G profile in Case 1 at $x \sim 55$ mm (Fig. 3(1)) is due to the delayed homogeneous ignition at the lower wall (see Fig. 2(1b)); the homogeneous ignition positions of Fig. 2 are also repeated in Fig. 3. The catalytic (C) conversion rates at positions upstream of any appreciable rise in gaseous (G) conversion are practically the same for all cases of Fig. 3 since the inlet Reynolds number is constant and the catalytic reactions are close to the mass-transport-limit. This allows for an initial qualitative comparison of the gaseous reactivities (given the differences in wall temperatures shown in Fig. 3). Figures 2 and 3 indicate a suppression of gaseous conversion with rising pressure and the reasons for this behavior are elaborated next.

4.2. Effect of pressure on hetero-/homogeneous chemistry

To address the impact of pressure on the hetero-/homogeneous processes, the pure homogeneous ignition characteristics of hydrogen are investigated first. Ignition delay times are provided in Fig. 5 for a $\varphi = 0.28$ H_2/air mixture. The gas-phase ignition delays were computed using CHEMKIN [25] at various constant temperatures in order to mimic the presence of the hot catalytic walls that heat the flowing reacting gas (the ignition delays were defined as the times required for hydrogen to drop to 50% of its initial concentration). At a moderate temperature of 950 K, the gaseous reactivity initially decreases (the ignition delay increases) rapidly with rising pressure, while above 2 bar it only changes modestly. At $T \geqslant 1000$ K, the reactivity initially increases with rising pressure and then drops, with the turning point shifted to higher pressures for higher temperatures. This rich behavior of hydrogen gaseous ignition characteristics is caused by the competition between the chain branching step $H + O_2 \Leftrightarrow O + OH$, the chain terminating step $H + O_2 + M \Leftrightarrow HO_2 + M$ (the latter is favored at low temperatures and high pressures) and also of the chain branching sequence $HO_2 + H_2 \Leftrightarrow H_2O_2 + H$ and $H_2O_2 + M \Leftrightarrow 2OH + M$ that overtakes the stability of HO_2 in the termination step [26]. The computed reaction rates for the cases of Fig. 2 indicate that for pressures above 2 bar the step $H_2O_2 + M \Leftrightarrow 2OH + M$ overtakes $H + O_2 \Leftrightarrow O + OH$ as the main OH producer (by a factor of 10 at 10 bar).

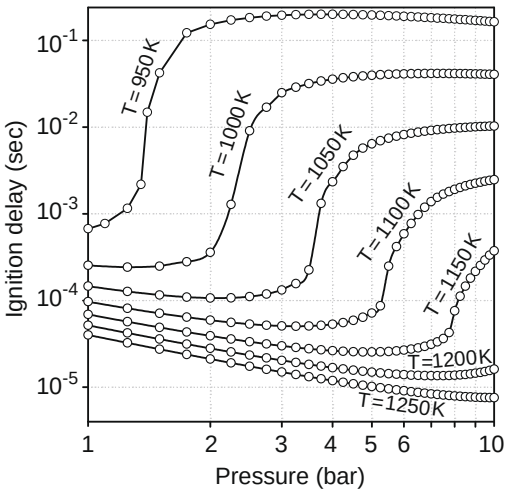

Fig. 5. Predicted ignition delays of a $\varphi = 0.28$ H_2/air mixture at different pressures and temperatures.

For the spatially inhomogeneous reactor of Fig. 1, the relevant effective temperatures of Fig. 5 are a weighted average between the inlet temperature (310 K) and the wall temperature (with added weight on the latter). For the current wall temperatures (between 1080 and 1200 K over the length $0 < x < 80$ mm wherein homogeneous ignition occurs), the resulting effective temperatures are moderate enough, such that the gaseous reactivity is highest at atmospheric pressure. The implication for a hetero-/homogeneous combustion system is that the catalytic pathway has the opportunity to consume significant amounts of hydrogen during the elongated high-pressure gas-phase induction zones, thus depriving fuel from the gaseous pathway and inhibiting homogeneous ignition. It is noted that the catalytic pathway is very effective in converting hydrogen due to the large molecular diffusivity of this species and its very high reactivity on Pt even at moderate surface temperatures (see the mass-transport-limited conversion in Fig. 4a).

The hetero-/homogeneous chemistry coupling is discussed next. It has been established in atmospheric pressure studies [14] that the hetero-/homogeneous radical (OH, O and H) coupling via adsorption/desorption reactions is weak. The same is also attested in the present high-pressure investigation: decreasing the radical adsorption/desorption rates by 20 and computing anew, has practically no effect on the predictions of Figs. 2 and 3. On the other hand, the impact of heterogeneously produced major species is profound. The catalytically produced H_2O is, over the gas-phase induction zone, as high as 22% vol. in the near-wall hot ignitable zones (Fig. 4a). Atmospheric pressure studies [14] have shown that the

catalytically produced water inhibits homogeneous ignition due to its high third body efficiency in the terminating step $H + O_2 + M \Leftrightarrow HO_2 + M$. This inhibition is much more pronounced at higher pressures. Figure 6 provides the transversely integrated gaseous hydrogen consumption rates for three cases of Fig. 2, computed by changing the efficiencies of H_2O in all reactions involving a third body from their nominal value (12 or 11, depending on the specific reaction) to the efficiency of nitrogen (unity). Comparisons of Figs. 6 and 3 indicate that strong homogeneous combustion is now established even at 10 bar. Therefore, the homogeneous combustion suppression at $p \geqslant 4$ bar bears the combined effects of the intrinsic hydrogen gaseous kinetics and also of the hetero-/homogeneous chemistry coupling via the catalytically produced H_2O.

The impact of transport is investigated numerically by artificially setting the diffusivity of H_2 equal to that of O_2. Fig. 7 provides the percentage of gas-phase H_2 conversion for normal and altered H_2 diffusivity. To facilitate the identification of transport effects, Fig. 7 pertains to the conditions of the following Section 4.3 whereby the same wall temperature was used at all pressures. It is evident that the high-diffusivity of H_2 decreases only mildly the limiting pressure for gas-phase combustion suppression (by ~1 bar, from 5 to 4 bar). Hence the dominant factor of gaseous combustion suppression is kinetics and not transport. It is noted, however, that transport is inherently coupled to the previously discussed kinetic inhibition mechanism via the catalytically produced H_2O: the H_2O near-wall content (~22% vol., see Fig. 4a) is roughly twice that occurring in pure homogeneous combustion ($\varphi = 0.28$ H_2/air), due to the diffusional imbalance of H_2 that results in an effective surface equivalence ratio about twice that of the gaseous phase [27].

4.3. Implications for practical reactors

In practical reactors the channel heights are smaller than the 7 mm of the optically accessible reactor. Computations have been carried out for a 1.5-mm height and 50-mm long channel with $T_{IN} = 723$ K, $Re_{IN} = 764$ (both values are typical of turbines) and constant wall temperature of 1250 K (a safe upper limit for long-term catalyst stability). The transversely integrated gaseous hydrogen reaction rates of Fig. 8 reveal that homogeneous combustion is again mostly suppressed for $p \geqslant 4$ bar. Despite the higher inlet and wall temperatures, the increased surface-to-volume ratio of this channel favors the catalytic hydrogen conversion and inhibits gaseous combustion at $p \geqslant 4$ bar. Interestingly, the hydrogen conversion reaches a maximum at 2 bar. This is attributed to a corresponding higher effective temperature in Fig. 5: the gas-phase reactivity initially increases, reaches a maximum at $p > 1$ bar, and afterwards decreases again (see e.g. the curve at 1050 K in Fig. 5).

The absence of appreciable gas-phase hydrogen conversion at $p \geqslant 4$ bar can be crucial in reactor design. Appel et al. [14,18] have shown that the presence of a flame is beneficial in moderating

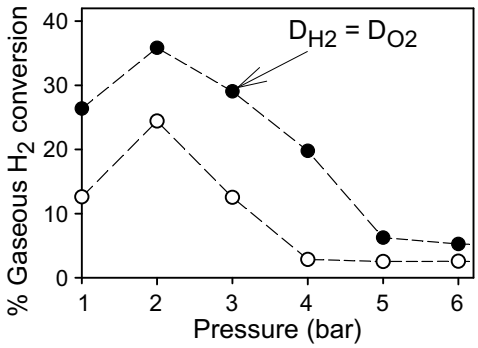

Fig. 7. Predicted percentage fraction of homogeneous hydrogen conversion (open circles) and same calculations for hydrogen diffusivity $D_{H2} = D_{O2}$ (filled circles). Operating conditions and geometry as in Fig. 8.

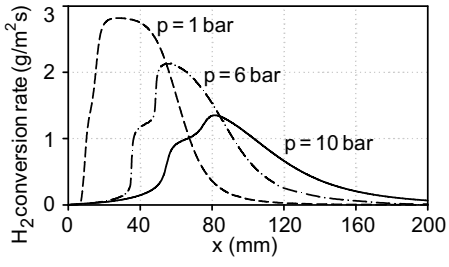

Fig. 6. Predicted axial profiles of transversely integrated gaseous hydrogen conversion rates for three cases of Fig. 2, with the third body efficiency of water set to unity.

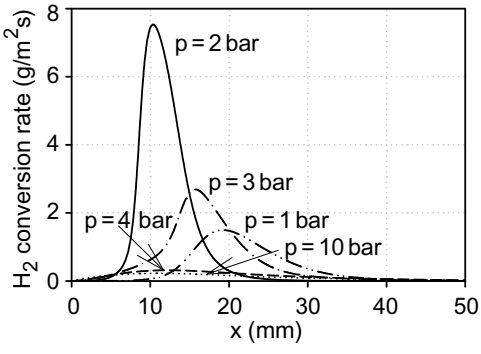

Fig. 8. Predicted axial profiles of y integrated gas-phase hydrogen conversion rates for a 1.5-mm height channel at five pressures: $\varphi = 0.28$, $T_{IN} = 723$ K, $T_W = 1250$ K and $Re_{IN} = 764$.

the reactor temperature by shielding the catalytic surfaces from the hydrogen-rich channel core and thus reducing the heterogeneous conversion that is responsible for the superadiabatic surface temperatures. The absence of this shield can be of concern for reactor thermal management at elevated pressures. On the other hand, for $p < 4$ bar the choice of a particular operational pressure can either enhance or reduce the contribution of gaseous chemistry depending on the reactor temperature. This very specific pressure dependence should be considered (along with other parameters, e.g. the geometrical confinement [28]) in the design of hydrogen microreactors.

5. Conclusions

The hetero-/homogeneous channel-flow combustion of fuel-lean hydrogen/air mixtures over Pt was studied at pressures up to 10 bar. In situ laser-based measurements, in conjunction with detailed 2-D numerical predictions, were used to investigate the catalytic and gas-phase chemical processes and their respective coupling. The employed hetero-/homogeneous chemical reaction schemes reproduced the measured catalytic fuel consumption and the onset of homogeneous ignition at pressures of up to 3 bar. Homogeneous combustion was largely suppressed at $p \geqslant 4$ bar due to the combined effects of the intrinsic gas-phase hydrogen kinetics and of the heterogeneously produced water acting as very efficient third body in radical gas-phase chain terminating reactions. Moreover, the impact of transport on the aforementioned gas-phase inhibition is modest. At practical reactor channel confinements, homogeneous combustion was still largely suppressed for $p \geqslant 4$ bar, even at the high inlet and wall temperatures of 723 and 1250 K, respectively. The suppression of gaseous combustion at high pressures is of particular concern for reactor thermal management since the presence of flames moderates the superadiabatic surface temperatures attained during the catalytic combustion of hydrogen.

Acknowledgment

Support was provided by the Swiss Federal Office of Energy (BFE) and ALSTOM Power of Switzerland.

Appendix A. Supplementary data

Supplementary data associated with this article can be found, in the online version, at doi:10.1016/j.proci.2008.06.067.

References

[1] H.M. Kvamsdal, K. Jordal, O. Bolland, *Energy* 32 (2007) 10–24.
[2] D.G. Norton, E.D. Wetzel, D.G. Vlachos, *Ind. Eng. Chem. Res.* 43 (2004) 4833–4840.
[3] D.G. Norton, D.G. Vlachos, *Proc. Combust. Inst.* 30 (2005) 2473–2480.
[4] R. Carroni, V. Schmidt, T. Griffin, *Catal. Today* 75 (2002) 287–295.
[5] K. Maruta, K. Takeda, J. Ahn, et al., *Proc. Combust. Inst.* 29 (2002) 957–963.
[6] D. Kyritsis, I. Guerrero-Arias, S. Roychoudhury, A. Gomez, *Proc. Combust. Inst.* 29 (2002) 965–972.
[7] S. Karagiannidis, J. Mantzaras, G. Jackson, K. Boulouchos, *Proc. Combust. Inst.* 31 (2007) 3309–3317.
[8] J. Li, Z. Zhao, A. Kazakov, F.L. Dryer, *Int. J. Chem. Kinet.* 36 (2004) 566–575.
[9] S.M. Walton, X. He, B.T. Zigler, M.S. Wooldridge, *Proc. Combust. Inst.* 31 (2007) 3147–3154.
[10] M. Reinke, J. Mantzaras, R. Bombach, S. Schenker, A. Inauen, *Combust. Flame* 141 (2005) 448–468.
[11] J. Mantzaras, in: S.Z. Jiang (Ed.), *Focus on Combustion Research*, Nova Publishers, New York, 2006, p. 241.
[12] U. Dogwiler, J. Mantzaras, P. Benz, et al., *Proc. Combust. Inst.* 27 (1998) 2275–2282.
[13] M. Reinke, J. Mantzaras, R. Schaeren, et al., *Combust. Flame* 136 (2004) 217–240.
[14] C. Appel, J. Mantzaras, R. Schaeren, et al., *Combust. Flame* 128 (2002) 340–368.
[15] M. Reinke, J. Mantzaras, R. Bombach, et al., *Combust. Sci. Technol.* 179 (2007) 553–600.
[16] A. Schneider, J. Mantzaras, R. Bombach, et al., *Proc. Combust. Inst.* 31 (2007) 1973–1981.
[17] W.C. Pfefferle, L.D. Pfefferle, *Prog. Energy Combust. Sci.* 12 (1986) 25–41.
[18] C. Appel, J. Mantzaras, R. Schaeren, R. Bombach, A. Inauen, *Combust. Flame* 140 (2005) 70–92.
[19] O. Deutschmann, R. Schmidt, F. Behrendt, J. Warnatz, *Proc. Combust. Inst.* 26 (1996) 1747–1754.
[20] J. Warnatz, M.D. Allendorf, R.J. Kee, M.E. Coltrin, *Combust. Flame* 96 (1994) 393–406.
[21] R.J. Kee, F.M. Rupley, J.A. Miller, *Chemkin II: A Fortran Chemical Kinetics Package for the Analysis of Gas-Phase Chemical Kinetics*, Report No. SAND89-8009B, Sandia National Laboratories, 1996.
[22] M.E. Coltrin, R.J. Kee, F.M. Rupley, *Surface Chemkin: A Fortran Package for Analyzing Heterogeneous Chemical Kinetics at the Solid Surface–Gas Phase Interface*, Report No. SAND908003C, Sandia National Laboratories, 1996.
[23] R.J. Kee, G. Dixon-Lewis, J. Warnatz, M.E. Coltrin, J.A. Miller, *A Fortran Computer Code Package for the Evaluation of Gas-Phase Multicomponent Transport Properties*, Report No. SAND868246, Sandia National Laboratories, 1996.
[24] J. Mantzaras, P. Benz, *Combust. Flame* 119 (1999) 455–472.
[25] A.E. Lutz, R.J. Kee, J.A. Miller, *SENKIN: A Fortran Program for Predicting Homogeneous Gas Phase Chemical Kinetics With Sensitivity Analysis*,

Report No. SAND87-8248, Sandia National Laboratories, 1996.
[26] I. Glassman, *Combustion*, Academic Press, London, 1996, p. 67.
[27] P.A. Bui, D.G. Vlachos, P.R. Westmoreland, *Proc. Combust. Inst.* 26 (1996) 1763–1770.
[28] J. Mantzaras, *Combust. Sci. Technol.* 180 (2008) 1137–1168.